Ultra-thin two-dimensional transmissive anisotropic metasurfaces for polarization filter and beam steering application*

Wen-Long Guo(郭文龙), Guang-Ming Wang(王光明)†, Hai-Peng Li(李海鹏), Kun Zhang(张昆), and Tong Cai(蔡通)

Air and Missile Defense College, Air Force Engineering University, Xi'an 710051, *China*

(Received 29 February 2016; revised manuscript received 20 April 2016; published online 25 August 2016)

We propose an anisotropic planar transmitting metasurface, which has the ability to manipulate orthogonally-polarized electromagnetic waves in the reflection and refraction modes respectively. The metasurface is composed of four layered rectangular patches spaced by three layered dielectric isolators each with a thickness of $0.15\lambda_0$ at 15 GHz. By tailoring the sizes of the patches, the metasurface functions as a band-stop filter for the *y*-polarzied wave and a band-pass filter for the *x*-polarized wave operating from 14 GHz to 16 GHz. Moreover the phases of the transmitting *x*-polarized wave can be modulated at about 15 GHz, which contributes to beam steering according to the general refraction law. Experimental results are in good accordance with the simulated ones, in which the reflection efficiency is almost 100% while the transmission efficiency of the *x*-polarized wave reaches 80% at 15 GHz. Besides, the transmitted *x*-polarized wave is effectively manipulated from 14 GHz to 16 GHz.

Keywords: metasurface, beam steering, polarization beam splitter

PACS: 41.20.Jb, 73.20.Mf **DOI:** 10.1088/1674-1056/25/10/104101

1. Introduction

Since Pendry *et al.*[1] and Smith *et al.*[2] proposed the concepts of negative permittivity and permeability, metamaterials have developed rapidly. In the research, the metasurface (MS),[3] a two-dimensional (2D) metamaterial composed of a subwavelength metamaterial unit cell,[4,5] has received the most attention due to its great flexibility in controlling the phase, amplitude and polarization status[6,7] of the transmitted/reflected electromagnetic (EM) waves. Especially, the ability of the metasurface to steer beams and manipulate the polarization state of the EM wave is more fascinating,[8–10] which has attracted numerous research. For example, based on the plasmonic response of the gold V-shaped nano-antenna, the beam steering according to the general refraction and reflection law in the optical spectrum was first proposed by Yu *et al*. in Ref. [3]. By tailoring cells on a nano-scale, the broadband linear conversion and anomalous refraction in the terahertz region were demonstrated in Ref. [11]. More recently the broadband circular and linear polarization conversions have been unanimously realized by employing a thin birefringent reflective metasurface.[12]

In addition, the independent controls of differently-polarized reflected waves by employing anisotropic metasurfaces have also been depicted.[13] Compared with the isotropic metasurfaces, the anisotropic ones have the advantage in polarization control and beam steering.[14] For instance, by using a Huygens metasurface the beam steering of orthogonally polarized transmitted waves was realized in Ref. [15]. By employing an anisotropic phase element, the transparent polarization beam splitter was also used in Ref. [16]. But note that the two papers mentioned above are both about beam steering for differently polarized transparent waves. Thus, an anisotropic metasurface with the function of polarization filter and beam steering still greatly needs to be studied.

In this paper, we propose an ultra-thin anisotropic transmitting measurface with band-stop and band-pass characteristics for x/y-polarized waves operating from 14 GHz to 16 GHz. Besides, the transmitted *x*-polarized waves can be flexibly modulated according to the general refraction law. The anisotropic metasurface element is investigated to find a broad bandwidth stopping the *y*-polarized wave propagating and enough phase range to manipulate the transmitted *x*-polarized waves. Good performances have been observed from both simulation and measurement results, which demonstrate the good capacity of the anisotropic metaurfaces to realize the function of polarization filter with beam steering in 14 GHz–16 GHz.

The rest of this paper is organized as follows. In Section 2 the design procedures for the anisotropic metasurface element are described. The beam steering properties of the polarization filter are investigated in Section 3 by designing a one-dimensional (1D) phase gradient metasurface. In Section 4, the simulation and measurement results are presented. Finally, some conclusions are drawn from the present study in the last section.

*Project supported by the National Natural Science Foundation of China (Grant No. 61372034).

†Corresponding author. E-mail: wgming01@sina.com

© 2016 Chinese Physical Society and IOP Publishing Ltd

2. Anisotropic transmitting element design

The anisotropic metasurface element is investigated from double layered rectangular patches spaced by a layered dielectric isolator with a thickness of $h = 1$ mm.

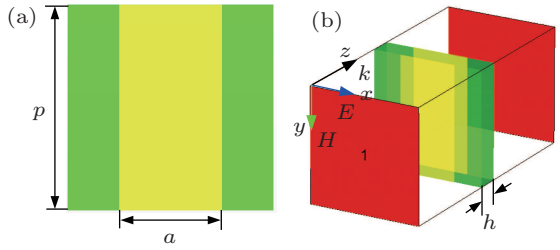


Fig. 1. (color online) Structure of the transmitted MS element and the simulated setup: (a) top view and (b) perspective view.

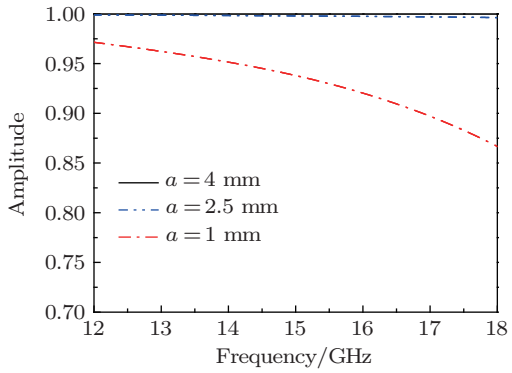


Fig. 2. (color online) Reflected efficiencies for y-polarized incident waves with the metasurface size a values of 4 mm, 2.5 mm, and 1 mm.

As shown in Fig. 1, in order to have the y-polarized beams reflected completely, the vertical length of the patch is set to be $p = 5$ mm, which is the same as the size of the dielectric substrate. The dielectric layer is with the dielectric constant $\varepsilon_r = 4.3$ and loss tangent 0.001. The horizontal length of the patch varies from 4 mm to 1 mm in order to investigate the reflected or the transmitted efficiency and the transmitted phase range.

Figure 2 depicts the reflected efficiency when the cell is impinged by the y-polarized wave. The conclusion can be drawn that the y-polarized beams are reflected completely with efficiency almost above 90% operating from 12 GHz to 18 GHz no matter how the variable a ranges. When impinged by the x-polarized wave, the phase element behaves as a low-pass filter with transmitted efficiency above 60% as depicted in Fig. 3(a). Moreover, as shown in Fig. 3(b), the phase range covers about 110° at 15 GHz with the variable x varying from 4 mm to 1 mm, which regrettably does not satisfy the requirement of the beam steering according to the general refraction law.[3] Fortunately, by employing multilayered resonance, the phase range covers 360° at 15 GHz with x varying from 4.1 mm to 1 mm when we set the metasurface element composed of four layered rectangular patches spaced by three layered dielectric isolators. Figure 5 depicts the reflected efficiencies of the double and triple layered element and figure 4 describes the transmitted efficiencies and phases of the double and triple layered element, clearly showing the band-stop and low-pass with phase controlling characteristic for x- and y-polarized waves.

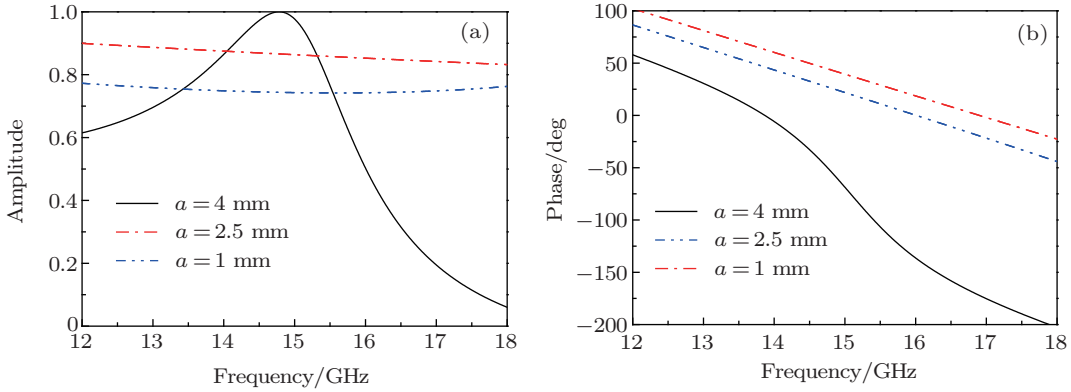
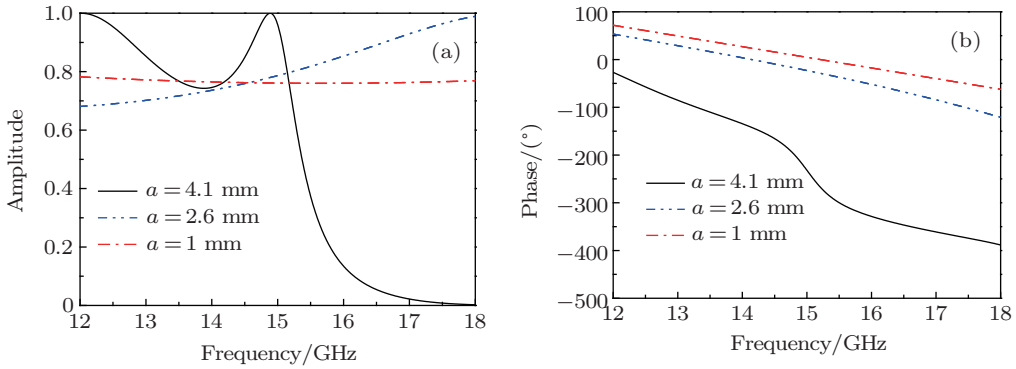


Fig. 3. (color online) (a) Transmitted efficiencies and (b) transmitting phase responses for x-polarized incident waves with the metasurface size a values of 4 mm, 2.5 mm, and 1 mm.



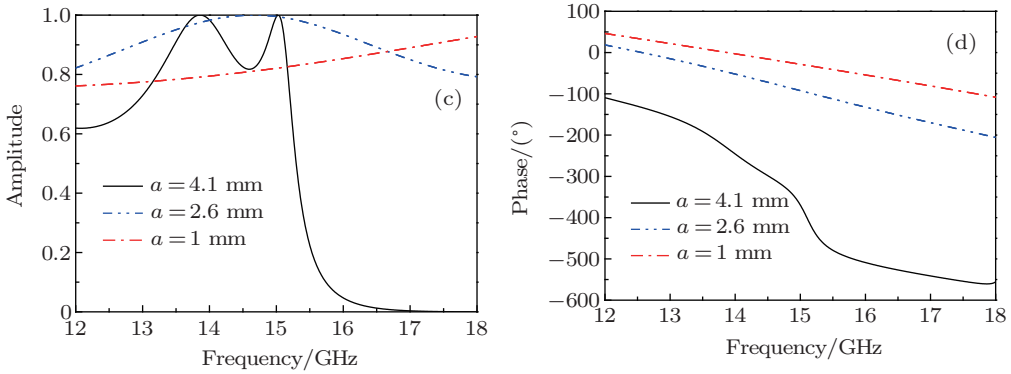


Fig. 4. (color online) (a) and (c) Transmitted efficiencies and (b) and (d) transmitting phase responses of the double and triple layered metasurface element for x-polarized incident waves with the variable a values of 4.1 mm, 2.6 mm, and 1 mm respectively.

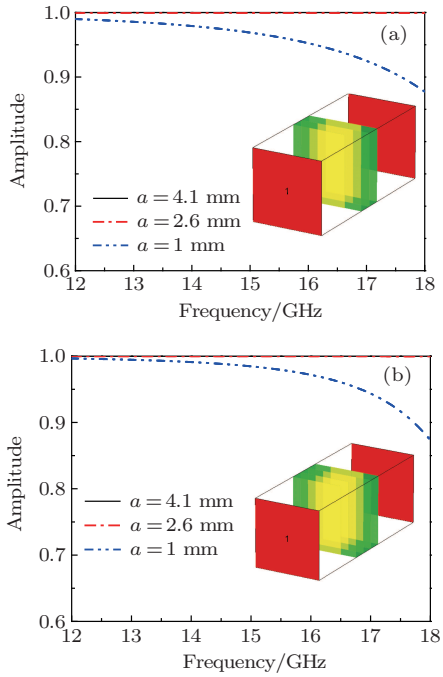


Fig. 5. (color online) Reflected efficiencies for y-polarized incident waves of (a) double layer and (b) triple layer metasurface element with a values of 4.1 mm, 2.5 mm, and 1 mm.

3. Design of 1D phase gradient metasurface

As shown in Fig. 6, on the basis of the triple layered cell we design a one-dimensional (1D) phase gradient metasurface (PGM) composed of six phase elements. In Fig. 7(d) are plotted the transmitted efficiency and absolute phase response for the distributed cells along the $+x$ axis at 15 GHz. The transmitted efficiency above 80% and a gradient phase of 60° can be observed. Besides, in order to detect the operating bandwidth of the PGM, the transmitted phase responses and efficiencies of the six cells operating in a frequency range of 14 GHz–16 GHz are also depicted in Figs. 7(a) and 7(b). Figure 7(c) shows the reflected efficiencies for the six cells also in a frequency range from 14 GHz to 16 GHz. From the elements constructing the PGM, we can conclude that the constituted PGM will effectively steer beams from 14 GHz to 16 GHz. As depicted in Fig. 6, the designed metasurface irradiated by the plane waves is simulated in CST Microwave Studio where periodic boundary conditions are assigned in x and y directions and an open boundary condition is set in the z direction. In Fig. 8 are plotted the reflection coefficients (S_{11}) for the case where the surface is impinged by x- and y-polarized waves respectively. It can be seen that the y-polarized waves are almost reflected completely while the x-polarized modes have access to transmitting through the surface operating in 14 GHz–16 GHz. In order to detect the working procedure of the metasurface, the E-field distributions at 15 GHz on the xoz plane under x- and y-polarized waves' illumination are shown in Figs. 9(a) and 9(b). Extraordinary refraction and normal reflection are obtained when the surface is impinged by x- and y-polarized waves respectively. The deflection angle of x-polarized refraction beams is displayed in Fig. 10, in which the colored graph correspond to the simulated refraction angles and the pentagrams correspond to the theoretical ones in a frequency range of 14 GHz–16 GHz. On a separate note, the graph describes the deflection angles on the xoz plane with the reference frame as depicted in Fig. 6.

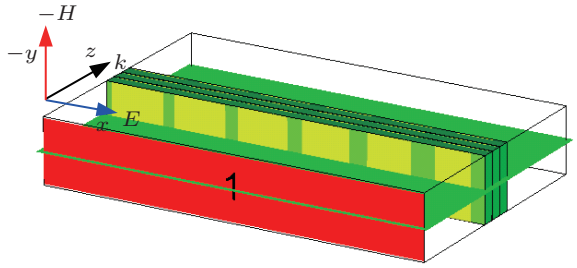


Fig. 6. (color online) Designed one-dimensional phase gradient metasurface and its simulation setup.

Obviously, the simulated deflection angles are in good accordance with the theoretical ones calculated by general refraction law as depicted below.[3]

$$n_{\mathrm{t}} \sin\theta_{\mathrm{t}} - n_{\mathrm{i}} \sin\theta_{\mathrm{i}} = \frac{\lambda}{2\pi} \frac{\mathrm{d}\Phi}{\mathrm{d}x}, \tag{1}$$

where n_{i} and n_{t} represent the refractive indices for the incident and the refractive medium, θ_{i} are θ_{t} are the incident and refractive angles, $\mathrm{d}\Phi$ corresponds to the phase gradient, and $\mathrm{d}x$ represents the size of the metasurface cell.

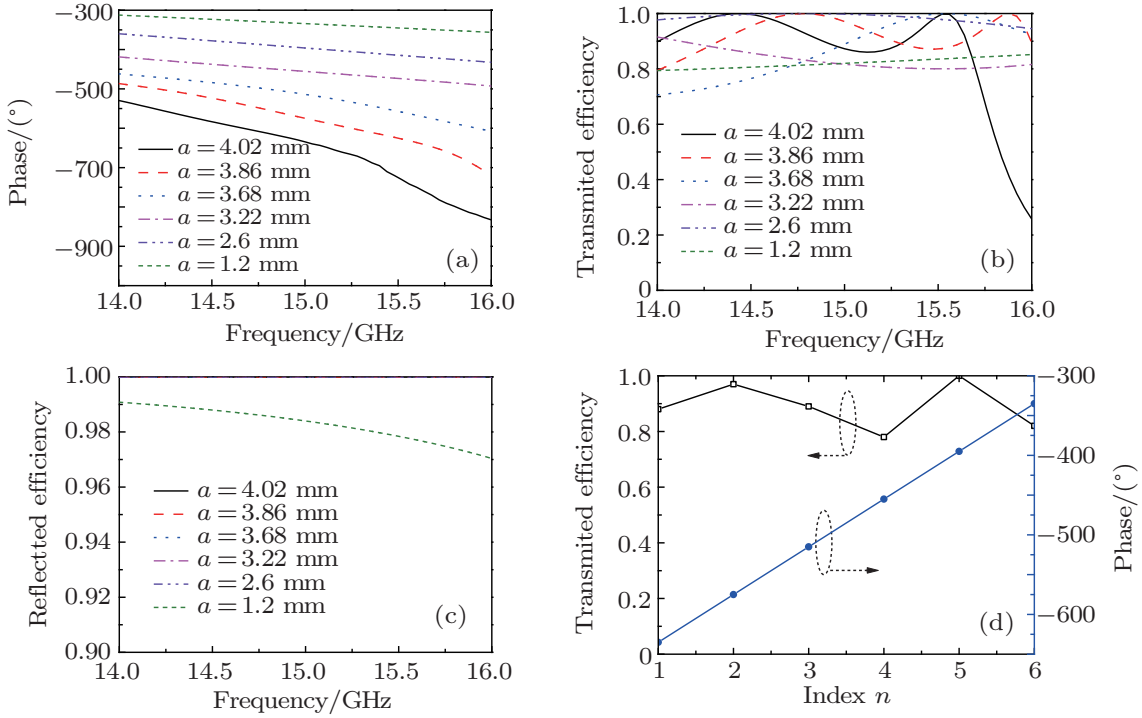


Fig. 7. (color online) (a) Phase shifts and (b) the transmitted efficiencies of the distributed cells under the irradiations of *x*-polarized waves in a frequency range of 14 GHz–16 GHz. (c) The reflected efficiencies of the six cells under the irradiations of *y*-polarized waves in a frequency range from 14G Hz to 16 GHz. (d) The transmitted efficiency and phase shift of the distributed cells at 15 GHz.

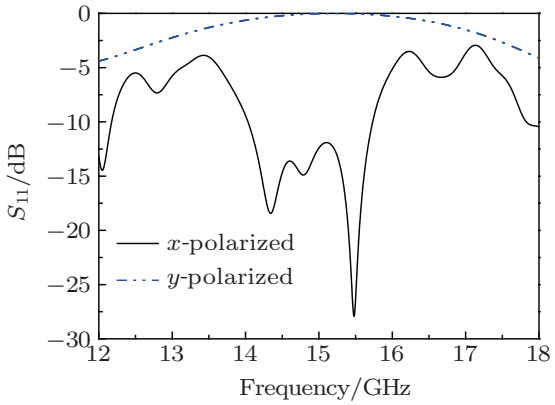


Fig. 8. (color online) Reflection coefficients of one-dimensional PGMS under the irradiations of *x*- and *y*-polarized waves.

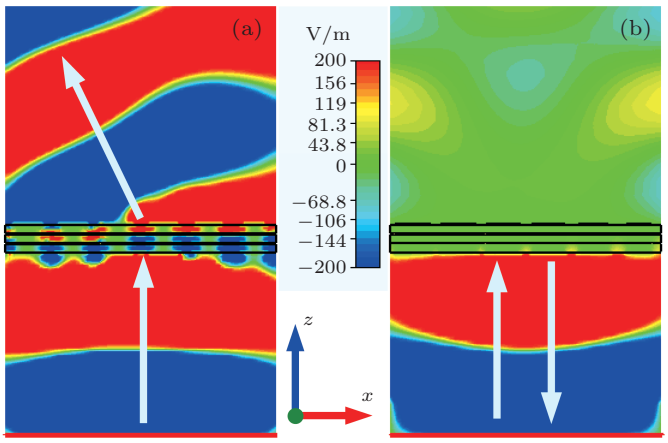


Fig. 9. (color online) *E* field distributions on the *xoz* plane under the irradiations of (a) *x*-polarized (b) *y*-polarized incident waves.

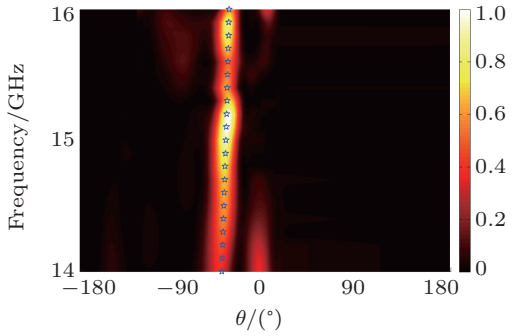


Fig. 10. (color online) Refraction angles corresponding to frequency range under the irradiation of *x*-polarized wave.

4. Anisotropic transmitting metasurface design and illustrative results

In order to further verify the design as shown in Fig. 11(a), we fabricate a metasurface sample composed of the supercells shown in Fig. 6 with a size of 210 mm×210 mm. When simulated in CST Microwave Studio and measured on the antenna test system in a microwave anechoic chamber, the sample is irradiated by waves with an incident angle of 15° in order to observe the reflection or refraction waves more conveniently. Besides, we make the horn antenna rotate in the way depicted in Fig. 11(b) to obtain the irradiations of differently polarized waves. The polarization state of incident wave can be described as

$$E = e_x|E|\sin\varphi + e_y|E|\cos\varphi. \tag{2}$$

Here, we set φ to be 0°, 90°, and 45° for obtaining *y*-,

x-, and x/y-polarized impinging waves and discuss the triple cases as illustrated below.

The first case taken into consideration is that the sample is irradiated by the y-polarized waves with a rotation angle set to be 0°. The fabricated sample is simulated and measured in the coordinate system as depicted in Fig. 12(a). By employing open boundary conditions on each side in CST, the E-field distribution on the xoz plane is calculated and demonstrated in Fig. 12(b), in which the incident y-polarized waves are all reflected normally. Besides, the far-field pattern of the constructed system at 15 GHz is simulated, measured and finally plotted in Fig. 13(a). The deflection angle of −165° can be observed at the position of peak gain, which is right opposite to the incident angle. That is to say, the far and near field results have both validated the normal reflection under the irradiations of y-polarized waves. To detect the operating bandwidth of the designed metasurface, the reflection angle in the xoz plane in a frequency range from 14 GHz to 16 GHz is plotted in Fig. 13(b), in which the colored graph corresponds to the simulated results and the pentagrams correspond to the measured results while the solid green line corresponds to the theoretical results. The conclusion can be drawn that the effective normal reflection operates in a frequency range of 14 GHz–16 GHz when the surface is irradiated by y-polarized waves.

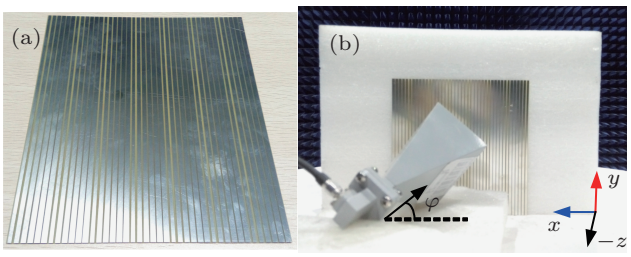


Fig. 11. (color online) (a) Top view of the fabricated metasurface sample and (b) the measured system with the horn antenna rotated to obtain differently polarized impinging waves.

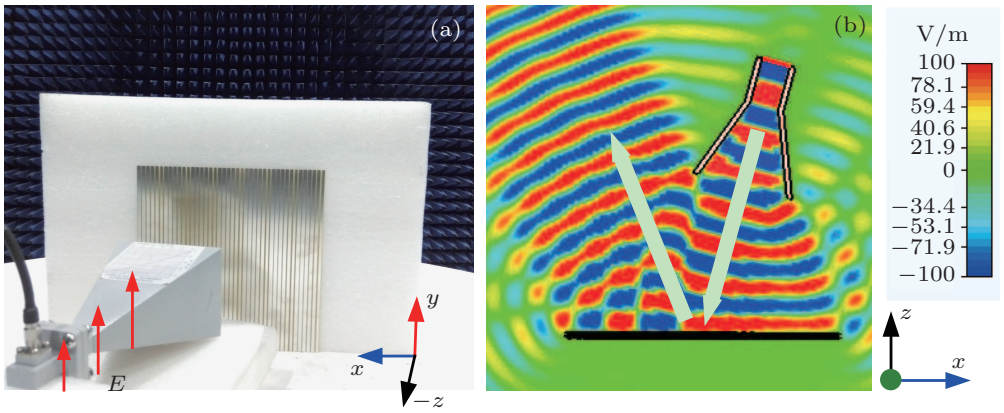


Fig. 12. (color online) (a) Measured view and (b) the E field distribution on the xoz plane of the metasurface sample under the irradiations of y-polarized waves.

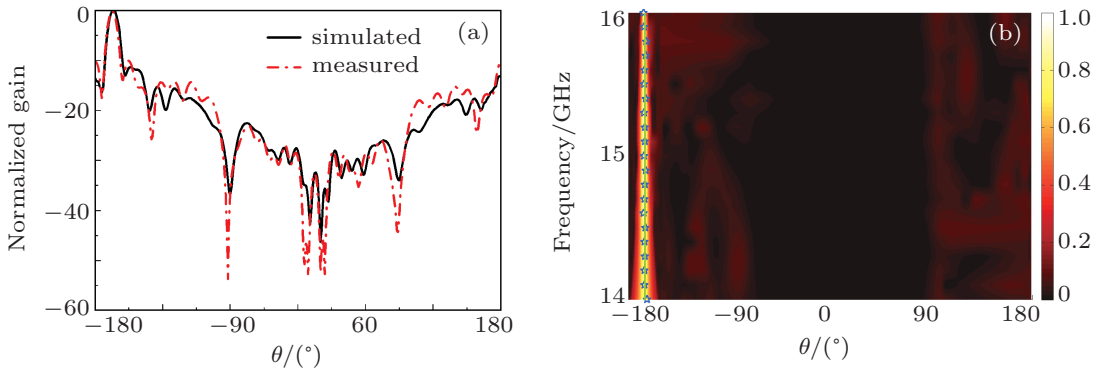


Fig. 13. (color online) (a) Normalized co-polarization far-field gains and (b) the deflection angles of the scattered beams on the xoz plane under the irradiations of y-polarized waves.

Then the horn antenna is rotated as shown in Fig. 14(a) in order to obtain the irradiations of x-polarized waves. The E-field distribution at 15 GHz on the xoz plane is also calculated as shown in Fig. 14(b). As arrowed in Fig. 14(b), anomalous refraction occurs when the surface is irradiated by x-polarized waves. Besides, figure 15(a) shows the simulated and measured co-polarization far-field patterns on the xoz plane, which further validate the anomalous reflection with a deflection angle of 24° at 15 GHz. In order to detect the sample operating bandwidth, we show the refraction angles on the xoz plane in a frequency range from 14 GHz to 16 GHz in Fig. 15(b). With significations of the colored graph, pentagram and the solid green line being identical to Fig. 13(b), the consistence between numerical and experimental results validates the effective anomalous refraction operating in a frequency range of 14 GHz–16 GHz.

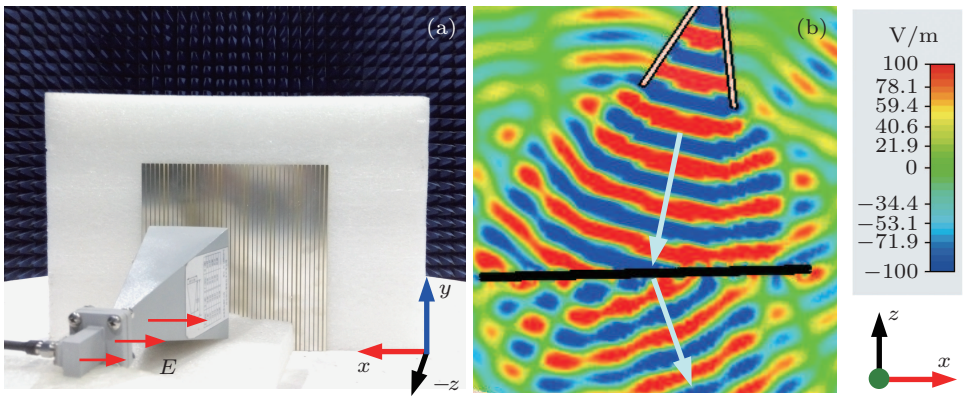


Fig. 14. (color online) (a) Measured view and (b) the E field distribution on the xoz plane of the metasurface sample under the irradiations of x-polarized waves.

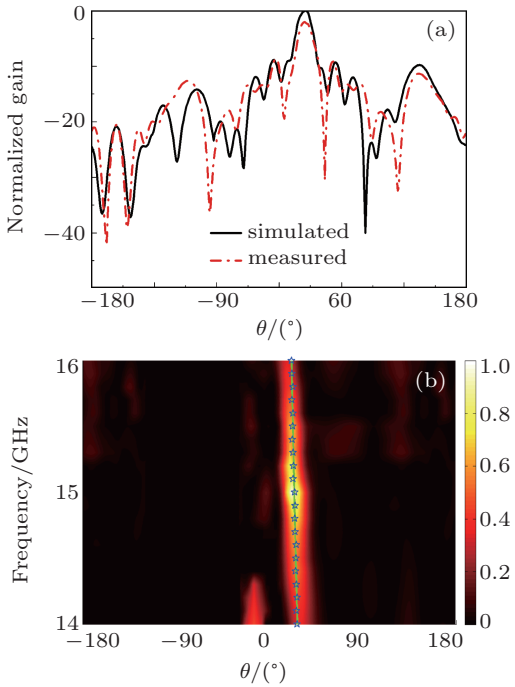


Fig. 15. (color online) Deflection angles of the scattered beams on the xoz plane under the irradiations of (a) y-polarized waves and (b) x-polarized waves.

Finally, by setting the horn antenna obliquely with $\varphi = 45°$ as shown in Fig. 11(b), the incident waves containing both x- and y-polarized waves impinge on the metasurface with an incident angle of 15°. The simulated and measured far-field patterns at 15 GHz are demonstrated in Fig. 16, where the deflection angles of x-polarized transmitting and y-polarized reflecting waves are in good accordance with the intended design values respectively. Furthermore, we depict the angles of the scattered beams on the xoz plane as shown in Fig. 17, in which the definitions of the colored, pentagram and solid green line are identical to those in Fig. 13. In addition, figures 17(a) and 17(b) show the scattered angles of x- and y-polarized waves respectively. With the simulated, measured and theoretical deflection angles being in good accordance, the metasurface sample has the ability to reflect the y-polarized waves normally and steer the refracted x-polarized waves flexibly according to the general refraction law in a frequency range of 14 GHz–16 GHz.

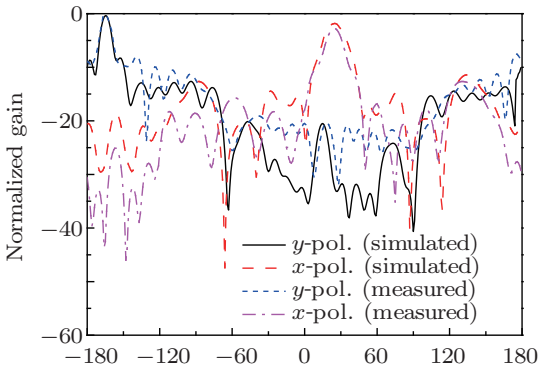


Fig. 16. (color online) Far-field patterns of the metasurface under the irradiations of x/y-polarized waves at an incident angle of 15° in the coordinate system shown in Fig. 13(b).

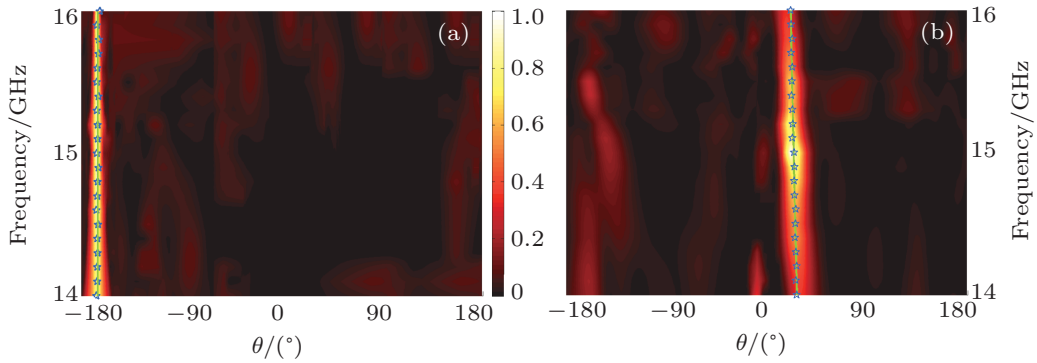


Fig. 17. (color online) Deflection angles corresponding to frequency range of (a) the x-polarized state and (b) the y-polarized state under the irradiations of x/y-polarized waves.

5. Conclusions and perspectives

In this study, we propose an anisotropic metasurface to obtain both polarization filter and anomalous refraction. This designed metasurface sample has the ability to reflect *y*-polarized waves completely and keep *x*-polarized modes not only transmitted but also manipulated operating in a frequency range from 14 GHz to 16 GHz. With the improvements in efficiency and the thickness reduction, this model has the potential application of realizing polarization filters or high-performance antennas.

Acknowledgment

The authors would like to express their gratitude to China's North Electronic Engineering Research Institute for fabricating the samples.

References

[1] Pendry J B, Holden A J, Robbins D J and Stewart W J 1998 *J. Phys.: Condens. Matter.* **10** 4785
[2] Smith D R, Padilla W J, Vier D C, Nemat-Nasser S C and Schultz S 2000 *Phys. Rev. Lett.* **84** 4184
[3] Yu N F, Genevet P, Kats M A, Aieta Francesco, Tetienne J P, Capasso F and Gaburro Z 2011 *Science* **334** 333
[4] Cheng J and Mosallaei H 2014 *Opt. Lett.* **39** 2719
[5] Chiya S and van der Daniel W 2015 *Appl. Phys. Lett.* **106** 113110
[6] Yang Q L, Gu J Q, Wang D Y, Zhang X Q, Tian Z, Ouyang C M, Ranjan S, Han J G and Zhang W L 2014 *Opt. Express* **22** 25931
[7] Zhang K, Ding X M, Zhang L and Wu Q 2014 *New J. Phys.* **16** 103020
[8] Li Y F, Zhang J Q, Qu S B, Wang J F, Wu X, Xu Z and Zhang A X 2015 *Acta Phys. Sin.* **64** 094101 (in Chinese)
[9] Sun S L, Yang K Y, Wang C M, Juan T K, Chen T K, Liao C Y, He Q, Xiao S Y, Kung W T, Guo G Y, Zhou L and Tsai D P 2012 *Nano Lett.* **12** 6223
[10] Li Y F, Zhang J Q, Qu S B, Wang J F, Zheng L, Zhou H, Xu Z and Zhang A X 2015 *Chin. Phys. B* **24** 014202
[11] Grady N K, Heyes J E, Chowdhury D R, Zeng Y, Reiten M T, Azad A K, Taylor A J, Dalvit D A R and Chen H T 2013 *Science* **340** 1304
[12] Ma H F, Wang G Z, Kong G S and Cui T J 2014 *Opt. Mater. Express* **4** 1717
[13] Ma H F, Wang G Z, Kong G S and Cui T J 2015 *Sci. Rep.* **5** 9605
[14] Zheng J, Ye Z C, Sun N L, Zhang R, Sheng Z M, Shieh H P D and Zhang J 2014 *Sci. Rep.* **4** 6491
[15] Jia S L, Wan X, Bao D, Zhao Y J and Cui T J 2015 *Laser Photon. Rev.* **9** 545
[16] Cai T, Wang G M, Zhang X F, Liang J G, Zhuang Y Q, Liu D and Xu H X 2015 *IEEE Trans. Anten. Propag.* **63** 5629